# Non-Fullerene Acceptor-Based Nanomorphology Enhancement for Efficient Ternary Organic Solar Cells

# Non-Fullerene Acceptor-Based Nanomorphology Enhancement for Efficient Ternary Organic Solar Cells

*Lubna Khanam,*[a] *Shashi Bhushan Srivastava,*[a,b] *Thu Trang Do,*[c,d] *Prashant Sonar,*[c,e*] *and Samarendra Pratap Singh*[a*]

[a] Department of Physics, Shiv Nadar University, Gautam Buddha Nagar, Uttar Pradesh, India-201314

[b] Bionics and Vision Lab, Department of Ophthalmology, Henry Ford Medical Group, 1 Ford Place, Detroit MI, USA

[c] School of Chemistry and Physics, Queensland University of Technology (QUT), 2 George Street, Brisbane, Queensland 4001, Australia

[d] Centre for Organic Photonics & Electronics, School of Chemistry and Molecular Biosciences, The University of Queensland, Brisbane, Queensland 4072, Australia

[e] Centre for Material Science, Queensland University of Technology, Brisbane Queensland 4001, Australia

*Corresponding author.
*E-mail address*: samarendra.singh@snu.edu.in (Samarendra P. Singh), sonar.prashant @qut.edu.au (Prashant Sonar)



## ABSTRACT

Recently, the ternary active layer-based organic solar cells have shown remarkable increment in the power conversion efficiency by utilizing the synergistic effect of complementary absorption, band alignment, and nano-scale morphology enhancement. Non-fullerene acceptors are an important class of functional materials for the improved performance of ternary organic solar cells due to their role in improvising the light absorption and the morphology of the active layer. Here, the non-fullerene (NF) molecule, NAI-FN-NAI (BO), is used as the third component in the bulk heterojunction of PTB7-Th: PC71BM to fabricate the ternary organic solar cell. The magical number of the composition i.e., 20% by weight of the NF in the ternary active layer resulted in the power conversion efficiency (PCE) of 8.1% devices which is almost 35% higher efficiency than PTB7-Th: PC71BM binary devices having the PCE of 6%. The enhanced efficiency is observed even though the lessened effect of complementary absorption and band alignment factors of the NF. We attribute such an

This article has been accepted for publication and undergone full peer review but has not been through the copyediting, typesetting, pagination and proofreading process, which may lead to differences between this version and the Version of Record. Please cite this article as doi: 10.1002/pssa.202200143.

improved efficiency in ternary devices to the nano-scale morphology enhancement. It could pave the way to realize the best possible bulk heterojunction blend to attain high power conversion efficiency close to inorganic counterparts.

Keywords: Non-fullerene Acceptors, Ternary Organic Solar Cells, Donor-Acceptor Small Molecule, Impedance Spectroscopy



## 1. Introduction

With the significant advancement in performance, organic solar cells (OSCs) are acknowledged as an emerging technology owing to their unique advantages such as environmental friendliness, lightweight, low cost, potential application in flexible devices, and facilitating large-area production by printing technique [1–4]. The power conversion efficiency (PCE) of OSCs strongly depends on the thin film morphology [5–8]. In addition, moderate light harvest in the binary blend photoactive layer of polymer donor and fullerene acceptor is also led to reducing the performance [9,10]. In binary blend organic solar cells (OSCs), a large proportion of incident photons cannot be utilized due to their wide optical bandgap, which prevents further improvement of the PCE [11,12]. Traditionally, tandem device strategy has been utilized to cover maximum UV-Vis absorption spectrum to capture the photons for enhancing power conversion efficiency but this method is expensive, involves several interfaces, selection of orthogonal solvents, and complex fabrication protocols [13–15]. Ternary blends, which combine three photovoltaic materials into one active layer, are an effective alternative to enhance the performance of the OSCs [16,17]. Ternary blend methods demonstrate great potential while maintaining the simplicity of the fabrication processing method in single-junction devices [18–20]. The concept of adding the third component into the binary system was established to enhance the performance of the devices by extending the light absorption region due to complementary absorption, resulting in high short-circuit current density. Additionally, it results in improved morphology of the photoactive layer leading to favorable recombination behavior of the charge carriers [21–23]. The ternary blend strategy can facilitate efficient charge transfer between components via selection of materials with appropriate energy levels [18].

Currently, there are two ways to make the ternary photoactive layer, either one donor/two acceptors (D:$A_1$:$A_2$, where D stands for polymer donor, $A_1$ is the host material, and $A_2$ is the ternary component) or two donor/one acceptor ($D_1$:$D_2$:A) and high-efficiency ternary OSCs with both configurations have been reported so far [24–26]. However, in multi-donors/acceptor

cases, the hassle of mixing two polymer donors occurs due to a lack of entropic driving force, and also the potential to have strong intermolecular attractions between polymer chains [27]. Therefore, the mixing of acceptors, in a donor: multi-acceptors approach has the potential to offer morphological advantages. [6,6]-Phenyl-$C_{61}$-butyric acid methyl ester ($PC_{61}BM$) and [6,6]-phenyl-C71-butyric acid methyl ester ($PC_{71}BM$) are the fullerene derivatives that have been widely used as an electron acceptor for binary blend OSCs because of their advantages of large electron affinity, high electron mobility, and isotropy of charge transport [28,29]. But many intrinsic limitations of fullerene derivatives such as weak absorption in the visible region and energy levels discrepancy between a donor and an acceptor cannot be eliminated [30]. In recent years, the design and synthesis of non-fullerene acceptors (NFAs) have drawn extensive research interest in the field of donor: multi-acceptor ternary blend OSCs, in which they are used as a ternary component [31]. Since fullerene acceptors are not capable of absorbing a significant region of the visible spectrum, whereas non-fullerene organic small molecular low bandgap acceptors have emerged to supplement the optical absorption profiles of fullerene derivatives [32]. Moreover, NFAs simultaneously realize easily tunable energy levels, bandgap, resulting in low energy loss, and high current generation [33–35]. Therefore, NFAs based ternary blend OSCs have become a simple and effective approach for improving the photovoltaic performance of OSCs [36]. Recently, the PCE of ternary organic solar cells (TOSCs) have reached 17.6% for a non-fullerene acceptor system for devices fabricated and characterized in inert environment [37,38]. These advancements have motivated further research into device performances and device physics, particularly for TOSCs fabricated and characterized in ambient environment.

In this study, we introduced a non-fullerene small molecule NAI-FN-NAI (BO) as the third component in a multi-acceptor ternary system, where the host binary blend is based on a donor polymer (PTB7-Th) and fullerene derivative ($PC_{71}BM$). The small molecule non-fullerene (NF) acceptor NAI-FN-NAI (BO), having two acceptor and one donor moieties, is designed following an acceptor−donor−acceptor−donor−acceptor (A1−D−A2−D−A1) molecular configuration with NAI as the end-capping acceptor (A1), FN as electron-withdrawing central (A2) group, and thiophene ring as a donor (D) unit. The NAI-FN-NAI (BO) is designed and synthesized by Sonar et al. [39] and the detailed synthesis and optoelectronic properties are already reported. The strong electron-withdrawing moieties (9-fluorenone) incorporated in the backbone of NAI-FN-NAI (BO) makes it a suitable and interesting candidate to be used as electron transporting material. Moreover, the blend morphology with a suitable phase separation is also a critical attribute for realizing a high PCE in the bulk heterojunction organic

solar cells. The NAI-FN-NAI (BO) into the PTB7-Th:$PC_{71}BM$ blend enhances charge transport, reduces trap-assisted recombination, and improves the morphology of the blend photoactive layer. The optimized OSCs based on ternary PTB7-Th:$PC_{71}BM$:NAI-FN-NAI (BO) blend demonstrate a higher PCE of 8.1% (average □ 7.9%) than 6% (average □ 5.7%) of the binary PTB7-Th:$PC_{71}BM$ devices. Further studies with the assistance of atomic force microscopy (AFM) and impedance spectroscopy have been performed. A small amount of NAI-FN-NAI (BO) (20%) in the ternary blend is helpful for $PC_{71}BM$ to form efficient electron-transport pathways. Consequently, the electron mobility is increased and the electron trap density is decreased in the ternary photoactive layer in comparison with PTB7-Th:$PC_{71}BM$ binary blend. Eventually, the impeded bimolecular recombination and augmented charge collection lead to an enhanced PCE in the ternary blend OSC devices [40].

## 2. Results and discussion

### 2.1. Device Architecture and Design Principle:

The photoactive layer of the ternary organic solar cell (OSC) is comprised of a donor polymer (PTB7-Th), a fullerene acceptor ($PC_{71}BM$), and a non-fullerene acceptor, NAI-FN-NAI (BO) (Fig. 1a). The chemical structures of these organic semiconductors are shown in the right panel of Fig. 1(a). We designed the set of experiments for fabricating the ternary devices comprised of PTB7-Th, $PC_{71}BM$, and NAI-FN-NAI (BO). Further, the ternary OSC devices are compared with the control binary OSC devices made up of PTB7-Th:$PC_{71}BM$ and PTB7-Th:NAI-FN-NAI(BO) bulk heterojunction photoactive layers. For the study, the inverted architecture of OSCs (left panel of Fig. 1a) is considered for both binary and ternary OSC devices keeping all the processing in the ambient condition. The ternary-blend advantageously forms a stepwise energy profile for effective photovoltaic effect (Fig. 1b). The work function of the ZnO thin film coated on ITO substrate has been measured using scanning kelvin probe microscopy (SKPM), which was found to be 4.2 eV, which is close to the value reported in the article.[41] After the light is absorbed by the photoactive layer, the generated excitons dissociate, and the electrons move towards the NAI-FN-NAI (BO) and $PC_{71}BM$, and holes move towards the PTB7-Th. We assume that the ternary blend with suitable band alignment, as shown in Fig. 1(b), can provide an extended network for electron transport and extraction due to the presence of strong electron-withdrawing capacity of NAI-FN-NAI (BO) non-fullerene small molecules.

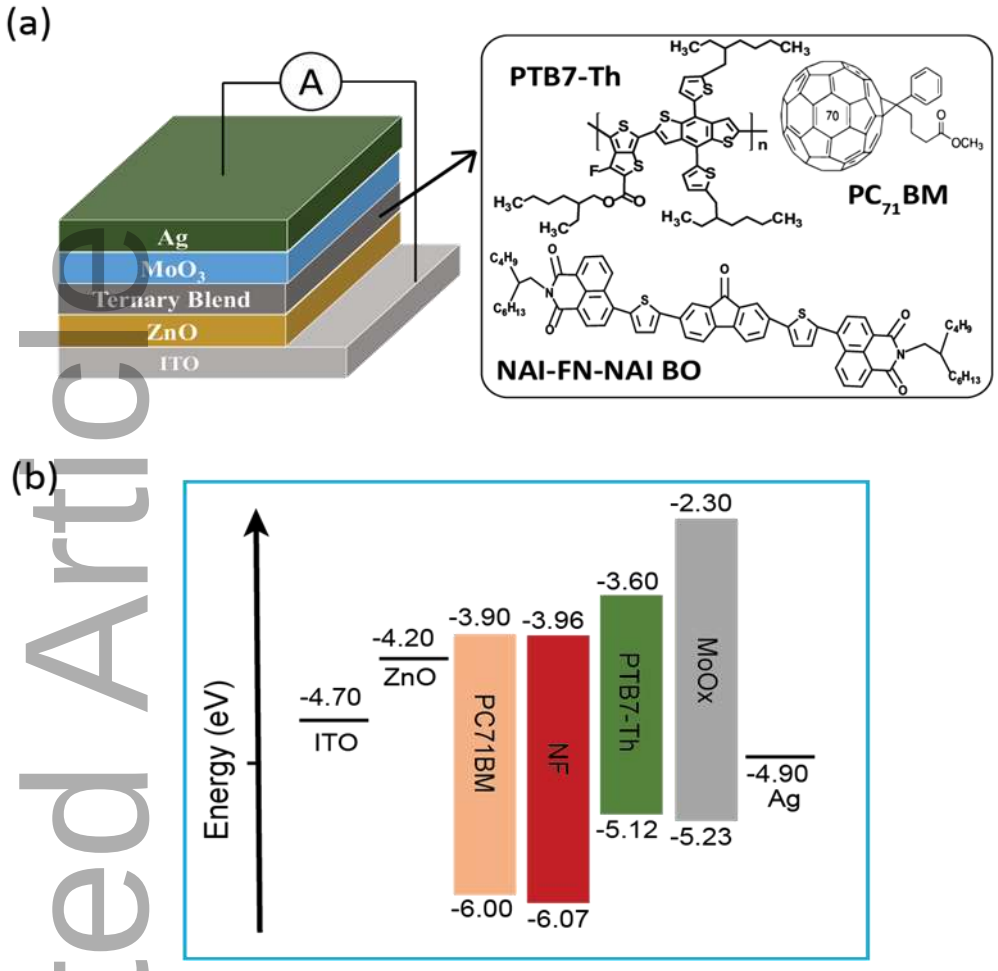


**Fig. 1.** (a) Right panel: Chemical structures of PTB7-Th, $PC_{71}BM$, and NAI-FN-NAI (BO), Left panel: Schematic showing the ternary (PTB7-Th: NAI-FN-NAI (BO): $PC_{71}BM$) bulk heterojunction photovoltaic device architecture, and (b) HOMO and LUMO energy levels of the components of the ternary organic solar cell and their band alignment for movement of the photogenerated charge carriers.



**2.2. Optical Analysis:**

The optical properties of the active layer constituents are critical to the OSC device performance which could provide insight into the photon conversion efficiency. Solutions of individual organic semiconductors are prepared in o-dichlorobenzene to perform UV-Vis absorption spectroscopy. Fig.

2(a) shows the typical absorbance of PTB7-Th and $PC_{71}BM$ solutions along with the absorption spectra of NAI-FN-NAI (BO) (NF). The absorption spectra of NAI-FN-NAI (BO) exhibit an absorption peak at 416 nm, matching with the previous report [39,42]. The Tauc plot of UV-Vis absorption spectra of PTB7-Th, $PC_{71}BM$, and NAI-FN-NAI (BO) solutions is shown in Fig. S5 (a), (b), and (c) in the supporting information to measure the optical band gap ($E_g$) which was found to be 1.65eV, 2.45eV, and 2.64eV respectively (determined as the x-intercept of the fit to the linear region). The absorption onset wavelength ($\lambda_{onset}$) is obtained as 770 nm, 545 nm, and 484 nm for PTB7-Th, $PC_{71}BM$, and NAI-FN-NAI (BO) respectively, by extending the linear part of the UV-Vis spectrum as shown in Fig. 2(d).[43,44]

The absorption spectra of binary and ternary active layer for different blend ratios of the fullerene and non-fullerene acceptors are shown in Fig. 2(b). The absorption peak of the control device (binary: PTB7-Th:$PC_{71}BM$) is found at 707 nm whereas it is red-shifted to 719 nm with slightly improved absorbance when 20% NF (of $PC_{71}BM$) is added to the ternary active layer. The red-shift and enhancement in the absorption are not linked to the NF introduction as it has absorbance in the blue region only. However, it could be an indication of the morphological changes due to the presence of crystalline NF small molecules.[42,45,46] Further, the ternary thin film with 50% of NF shows the reduction in absorbance peak of PTB7-Th. Moreover, it remains similar to the absorbance at the peak wavelength of the control device when the binary thin film was prepared using PTB7-Th and NF, as expected. However, the peak at 485 nm for the control device has a systematic blue shift with blend ratios of the fullerene and non-fullerene and resulted in 40 nm of maximum shift corresponding to the binary thin film only with NF molecules. The observed shift can be dedicated to the strong absorption of NF molecules with a peak at 407 nm.

The steady-state photoluminescence (PL) measurement is performed (in the solution) under the LED light excitation of 380 nm, 450 nm, and 417 nm respectively for PTB7-Th, $PC_{71}BM$, and NAI-FN-NAI (BO). For the binary and ternary blends, the excitation wavelength was 450 nm (Fig. 2d). It is observed that the neat PTB7-Th has shown a narrow emission peak at 757 nm wavelength, whereas neat NF material has shown a strong emission peak at 594 nm wavelength when compared to PTB7-Th and $PC_{71}BM$ with a weak emission peak at 756 nm wavelength. The emission intensity of PTB7-Th is almost completely quenched in the control blend solution. However, a systematic increase in the intensity of PTB7-Th with the inclusion of NF in different ratios in the blend solution suggests the lower quenching effect of PTB7-Th due to NF [47]. It can be confirmed from the lower quenching phenomenon observed in the case of a binary solution of the PTB7-Th and NF in the same ratio as it was in the control solution.

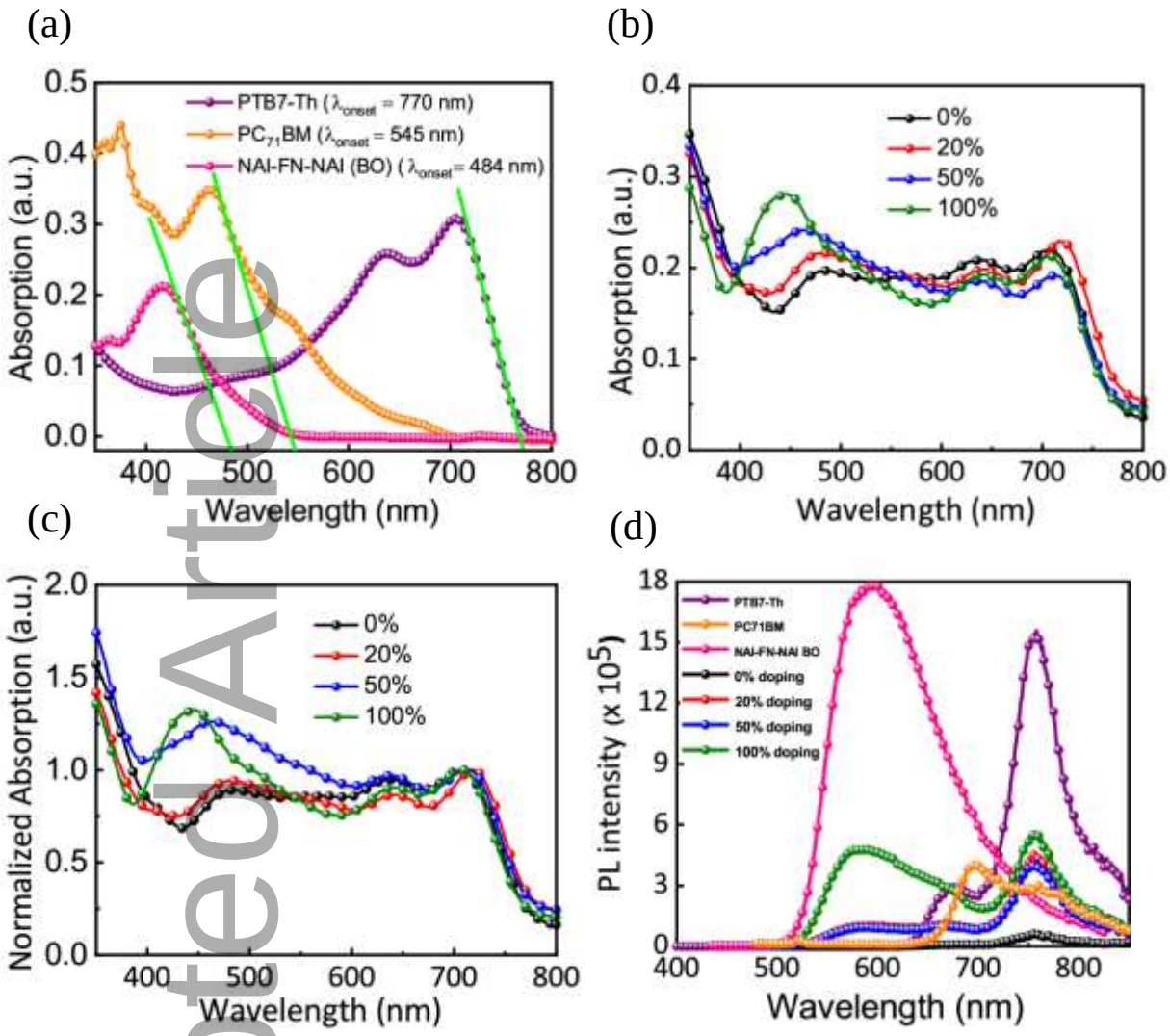


**Fig. 2.** UV-Vis absorption spectra for (a) PTB7-Th, $PC_{71}BM$, and NAI-FN-NAI (BO) solutions, (b) Binary and ternary active layer thin films, (c) Normalized (at 707 nm) UV-Vis absorption spectra, and (d) PL spectra of individual materials, binary, and ternary blend solutions.



**2.3. Solar Cell Characterization:**

Ternary BHJ organic solar cells (OSCs) based on PTB7-Th:$PC_{71}BM$ with different NAI-FN-NAI (BO) was fabricated with an inverted device architecture ITO/ZnO/PTB7-Th:NAI-FN-NAI (BO):$PC_{71}BM$/$MoO_x$/Ag in ambient condition. The performance of ternary devices is compared with the control binary device made-up of PTB7-Th:$PC_{71}BM$ BHJ in an inverted

device configuration ITO/ZnO/PTB7-Th:$PC_{71}BM$/$MoO_x$/Ag under similar condition. Additionally, the binary device with PTB7-Th:NAI-FN-NAI (BO) BHJ is also prepared in an inverted manner as ITO/ZnO/PTB7-Th:NAI-FN-NAI (BO)/$MoO_x$/Ag in the ambient condition. All the devices were characterized for current (I)-voltage (V) under solar simulation with 1.5 AM global radiation and 100 $mW.cm^{-2}$ light intensity (Fig. 3a). The ternary device with 20% NF has shown the highest power conversion efficiency (PCE) of 8.1% exhibiting the short-circuit current density ($J_{SC}$) of 15.4 $mA.cm^{-2}$ and the fill factor (FF) of 63.1% with low series resistance (6.8 $\Omega$-$cm^2$) and high shunt resistance (479.0 $\Omega$-$cm^2$). The improvement in all device parameters including parasitic resistances is observed in the ternary device with 20% NF when compared to the control binary device performance (PCE=6.0%, $J_{SC}$=12.7 $mA.cm^{-2}$, FF=53.1%, $R_S$=10.0 $\Omega$-$cm^2$, $R_{sh}$=216.7 $\Omega$-$cm^2$). However, we observed a slight reduction in the open-circuit voltage ($V_{OC}$) for the ternary device with 20% NF (0.83V) than the control device (0.87V) which can be explained by the reduction in the difference between the HOMO energy level of PTB7-Th and LUMO energy level of the NF (Fig. 1b). Further increase of NF percentage in the ternary composition led to the decrease of the device performance (Table 1) mainly because of a significant increase in the series resistance. It further resulted in a negligible performance of the binary device with 100% NF as acceptor material in the bulk heterojunction. The major difference between 20% NF devices and control binary devices is attributed to the fill factor enhancement and this could be due to the higher electron mobility enhancement due to two acceptor components [NAI-FN-NAI (BO) and $PC_{71}BM$] which is balancing with a hole mobility of PTB7-Th. It has been demonstrated that naphthalimide end capped anthraquinone based solution-processable organic semiconductor which is analogous to the NAI-FN-NAI (BO) exhibits electron mobility in organic transistor devices [48].

In an attempt to understand the physical mechanism of charge transport, we measured the capacitance-voltage (C-V) and impedance characteristics of the devices. The C-V analysis for the devices was performed for applied bias voltage range of -1 V to 1 V under dark conditions. The AC amplitude was kept at 10 $mV_{rms}$ to maintain the linearity of the response, and the measuring frequency was fixed at 5 kHz. The $C^{-2}$-V plot for binary and ternary devices is shown in Fig. 3(b). Classical Mott-Schottky (MS) analysis was applied to calculate the built-in-voltage ($V_{bi}$) and total acceptor charge carrier concentration ($N_A$) [49]. The $V_{bi}$ and $N_A$ for the devices under dark conditions are reported in Table 2. The $V_{bi}$ reduces to 0.65 V for 20% NF device as compared to 1.00 V for the control device. There is a decreasing trend in $V_{bi}$ with the increasing NF component in the ternary device and reached the lowest $V_{bi}$ for the

binary device with 100% NF. Simultaneously, $N_A$ decreased from $4.4 \times 10^{16}$ $cm^{-3}$ (for control device) to $2.4 \times 10^{16}$ $cm^{-3}$ for 20% NF ternary device and then starts increasing with the increase in NF percentage in the device. The observed changes in $V_{bi}$ and $N_A$ of these devices can be attributed to the interface modification between the cathode buffer layer (CBL) and organic active layer which explains the high performance of 20% NF-based ternary OPV device.

Further, we used impedance spectroscopy (IS) to investigate recombination of charge carriers and charge collection efficiency at the interfaces in the devices under working conditions. An externally applied alternating current (AC) signal can be used to probe non-radiative recombinations of charge carriers and charge transport in the devices. Here, an AC signal of amplitude 10 $mV_{rms}$ and frequency ranging from 1 Hz to 1 MHz with no DC offset has been utilized to perform the impedance spectroscopy of the devices. The Nyquist plot of the devices measured under dark is shown in Fig. 3(c) with scatter points. Further, to extract the underlying electrical parameters, the IS data has been fitted to a circuit model, proposed by Bisquert et al, consisting of electrical elements representing the various physical processes in the devices [50–52]. The solid lines in Fig. 3(c) represent the fitting curves to the IS data. The physical parameters estimated from the fitting of Nyquist plots agree with the experimental data. It is found that adding 20% NAI-FN-NAI (BO) into the PTB7-Th:$PC_{71}BM$ system can significantly decrease the series resistance ($R_S$) from 73.8 Ω to 45.9 Ω and increase the recombination resistance ($R_{rec}$) from 32 to 37.9 Ω. The $R_S$ further increased with increasing the doping concentration, and the maximum value of 226 Ω is obtained for 100%. Moreover, the $R_{rec}$ is further decreased with 50% doping but increased for 100% doping. The result indicates that the PCE enhancement for 20% ternary devices can be attributed to small $R_S$ along with the high $R_{rec}$. However, high $R_{rec}$ and $R_S$ were observed for the binary (100% NF content) device which could be the cause of the poor performance of PTB7-Th:NF binary device

However, high $R_{rec}$ and $R_S$ were observed for the binary (100% NF content) device which could be the cause of the poor performance of PTB7-Th:NF binary device [42].

Further, using the impedance data, reported in Table 3, the device performance was analyzed in terms of the charge collection efficiency for the binary and ternary blend devices. The charge collection efficiency depends on the ratio of electron diffusion length ($L_n$) to the blend layer thickness (L), which equals $(R_{rec}/R_t)^{1/2}$. Higher the value of $L_n/L$, the better the charge carrier collection at zero bias [40,53–56]. The calculated $(R_{rec}/R_t)^{1/2}$ parameter for the 20% NF device is higher than the 0% and 50% NF devices, in agreement with FF and PCE of the device. However, the devices with 100% NF show a much higher value of $(R_{rec}/R_t)^{1/2}$ which

indicates the better diode, but high series resistance depleted the power generation capacity of the device. An improvement in the charge collection efficiency in 20% NF device can be inferred by the higher values of $(R_{rec}/R_t)^{1/2}$ which can be attributed to the interface modulation as indicated in the CV analysis. The effective lifetime is low for the 20% NF device, but the electron mobility was observed to be significantly high for the 20% NF device leading to the $\mu.\tau$ product for the 20% NF OSCs being higher ($2.29\times 10^{-8}$) than the other ternary devices. These observations hint at an improved BHJ morphology [49,52]. It is known that the larger the $\mu.\tau$ value, the larger the carrier collection in the OSC devices. However, the link between the PCE and $\mu.\tau$ parameters depends on the nanoscale morphology of the active layer, contact resistance, and the configuration of the devices.[57] The effective lifetime is low for the 20% NF device but the electron mobility was observed to be significantly high and the product of $\mu.\tau$ was found to be $2.29\times 10^{-8}$ $cm^2/V$. However, with 100 % doping of NAI-FN-NAI (BO) $\mu.\tau$ product is maximum but the performance of the device is minimum due to the crystalline nature of the NF material, resulting in an increase in the series resistance of the devices. In general, the increased crystallinity of a semiconductor material should reduce the series resistance for a photovoltaic device but it is reversed in the case of a bulk heterojunction where the donor-acceptor interface is the primary criteria for the charge separation. Consequently, the devices show decreased PCE.

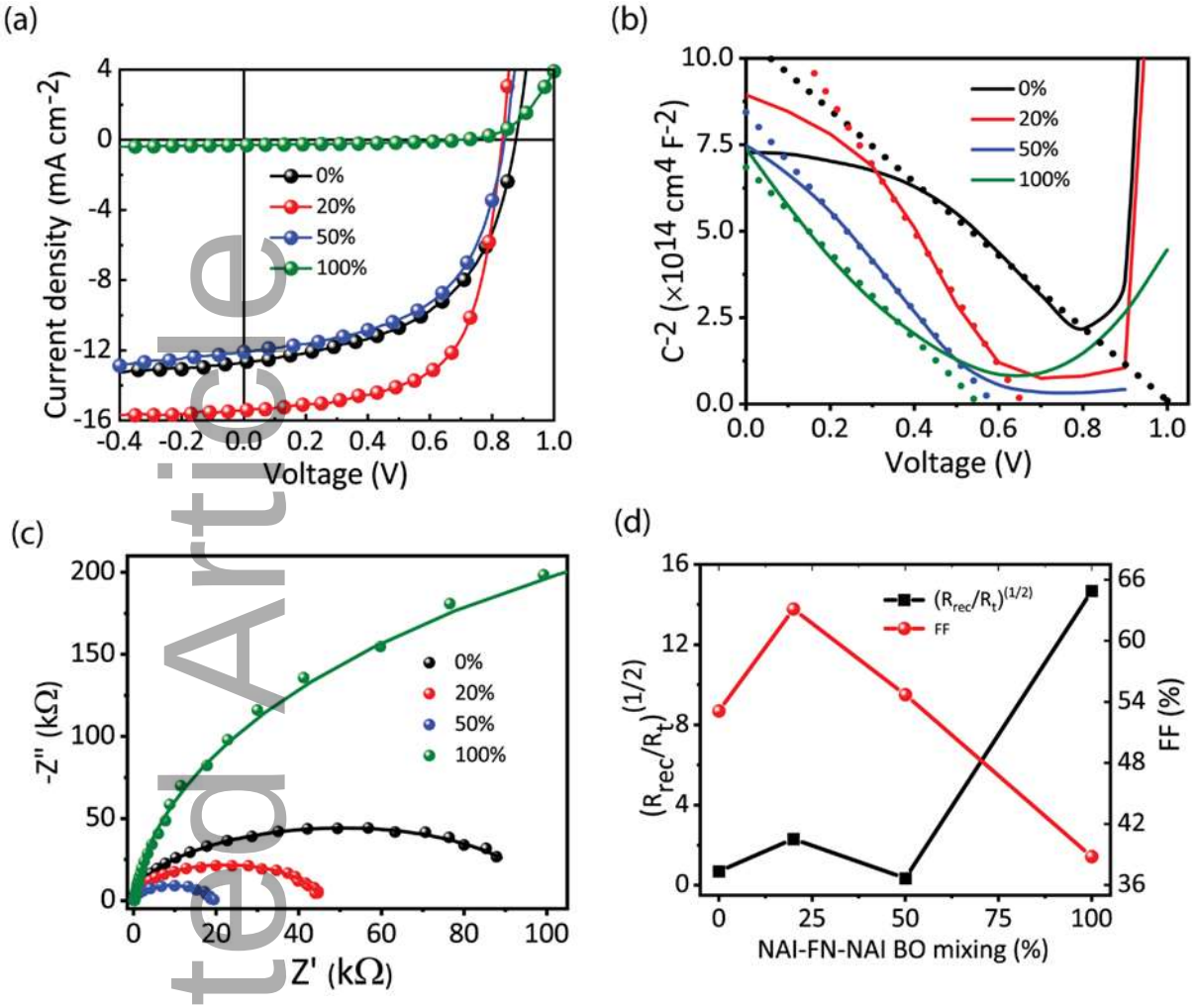


**Fig. 3.** (a) J-V characteristics of binary and ternary OSCs devices, (b) Mott-schottky plots of binary and ternary devices measured under dark condition keeping frequency at 5kHz, (c) Nyquist plots of impedance spectra for binary and ternary blend devices under dark at zero external dc voltage. Dots represent the experimental data and solid lines represent the fitting, and (d) $(R_{rec}/R_t)^{(1/2)}$ and FF with respect to the various mixing percentage of NAI-FN-NAI (BO) content in binary and ternary devices.



**Table 1.** The electrical parameters of binary and ternary OSCs at different NAI-FN-NAI (BO) content under 1000 W $m^{-2}$ illumination at AM1.5G in ambient condition.

| NAI-FN-NAI (BO) | $J_{sc}$ [mA.cm$^{-2}$] | $V_{oc}$ [V] | FF [%] | η [%] | $R_s$ [Ω-cm$^2$] | $R_{sh}$ [Ω-cm$^2$] |
|---|---|---|---|---|---|---|

| | | | | | | |
|---|---|---|---|---|---|---|
| **0%** | 12.7 | 0.87 | 53.1 | 6.0 [5.15±0.52] | 10.0 | 216.7 |
| **20%** | 15.4 | 0.83 | 63.1 | 8.1 [7.65±0.47] | 6.8 | 479.0 |
| **50%** | 12.1 | 0.84 | 54.7 | 5.6 [4.96±0.68] | 17.3 | 423.1 |
| **100%** | 0.3 | 0.68 | 38.8 | 0.08 [0.06±0.02] | 283.8 | 4277.5 |

**Table 2.** Built-in potential and total acceptor carrier concentration for binary and ternary blend devices from Mott-Schottky analysis.

| **Parameters** | **NAI-FN-NAI (BO) Doping Percentage** | | | |
|---|---|---|---|---|
| | **0%** | **20%** | **50%** | **100%** |
| **$V_{bi}$ [V]** | 1.00 | 0.65 | 0.58 | 0.55 |
| **$N_A$ [$cm^{-3}$]** | $4.4 \times 10^{16}$ | $2.4 \times 10^{16}$ | $3.2 \times 10^{16}$ | $3.8 \times 10^{16}$ |

**Table 3.** Electrical parameters of OSC devices are obtained from the IS study for binary and ternary blend devices.

| **Parameters** | **NAI-FN-NAI (BO) Doping Percentage** | | | |
|---|---|---|---|---|
| | **0%** | **20%** | **50%** | **100%** |
| **Series resistance (Ω)** | 73.8 | 45.9 | 62 | 226 |
| **Recombination resistance (kΩ)** | 32 | 37.9 | 2.01 | 536 |
| **Capacitance (nF)** | 3.11 | 2.87 | 2.83 | 2.52 |
| **Effective lifetime (μs)** | 244 | 2.79 | 14 | 582 |
| **Electron mobility ($cm^2$/V-sec)** | $8.54\times 10^{-6}$ | $8.20\times 10^{-3}$ | $3.70\times 10^{-5}$ | $1.60\times 10^{-3}$ |
| **$(R_{rec}/R_t)^{1/2}$** | 0.692 | 2.303 | 0.347 | 14.671 |



### 2.4. Surface Morphology:

The significant improvement (□ 35%) in the PCE for 20% NF containing ternary compared to the control device even though smaller contribution from the absorption and band alignment due to the introduction of NF acceptor. The analysis of the impedance and C-V measurements indicates the change in nanomorphology in the bulk heterojunction when crystalline NF

molecules are introduced as the third component of the ternary composition. The morphology of the active layer blend plays an important role in the improvement in the exciton diffusion, exciton separation, exciton recombination, and charge transport to the respective electrodes [58]. The effect of bulk heterojunction (BHJ) surface morphology on photocurrent is investigated for binary and ternary active layers. Fig. 4 shows the AFM images of 2 μm × 2 μm area of optimized ternary BHJ surfaces with varying NF loading and then compared with the control sample (binary BHJ) on ITO/ZnO coated glass substrates. The surface morphology of the control binary device shows an average roughness of 1.4 nm with smaller domains. However, a similar degree of average roughness (1.3 nm) is observed on the surface of the 20% NF ternary thin films with bigger clusters (Fig. 4b). Even though the surface roughness of the 20% NF device is similar to the control device, it has higher performance which can be attributed to the homogeneous distribution of different phases [39,42]. Due to improved morphological changes in 20% NF device which collectively affect exciton diffusion, exciton dissociation, and charge transport, fill factor and charge collection efficiency increased as compared to the reference device [59]. On the contrary, the surface roughness significantly increases with the increase in the NF percentage in the BHJ. It can be attributed to the higher crystallinity of NF molecules. High roughness results in a high leakage current which lowers the shunt resistance. Typically, the ternary component enhances the PCE of OSC devices structurally by acting as a template to facilitate supramolecular assembly in the blend film for achieving the ideal BHJ nanomorphology and electronically acting as an energy transfer agent to favor charge dissociation and transport.[60,61] The cascade energy level of the device is depicted in Fig. 1(b). For the binary device with 0% doping, exciton dissociation and charge carrier transfer occur at PTB7-Th/$PC_{71}BM$ interface due to the offset between the energy level of materials. However, PTB7-Th/NAI-FN-NAI (BO), and NAI-FN-NAI (BO)/$PC_{71}BM$ interface along with the PTB7-Th/$PC_{71}BM$ interface in ternary devices also assist in effective exciton dissociation and charge carrier transfer which results in the increment of the $J_{sc}$. The decrement in $J_{sc}$ and PCE for the 50% and 100% doping concentration can be attributed to the increment in the $R_s$ having a negative effect on the charge carrier transport, which is supported by the impedance study.

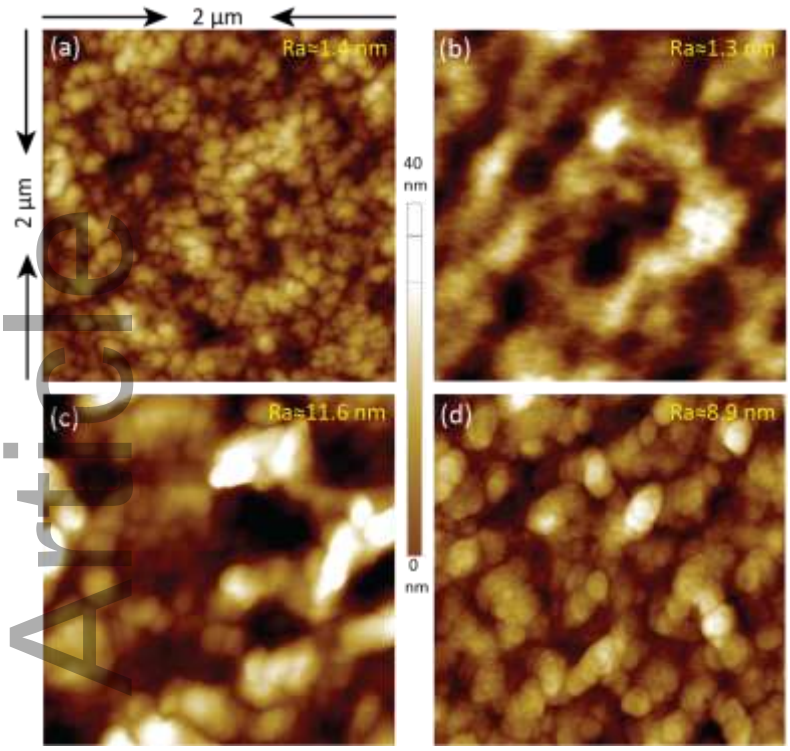


**Fig. 4.** AFM height images of the binary and ternary thin film, (a) binary blend thin film of PTB7-Th:$PC_{71}BM$, (b) PTB7-Th:$PC_{71}BM$:NAI-FN-NAI (BO) ternary blend film with 20% doping, (c) 50% doping, and (d) 100% doping.

## 3. Experimental

### 3.1. Materials

PTB7-Th, $PC_{71}BM$, and ITO were purchased from Luminescence Technology Corporation (Taiwan) and used as received. Non-fullerene acceptor, NAI-FN-NAI (BO) was synthesized by Sonar et al. [42]. Other reagents and chemicals were bought from Sigma-Aldrich and used as received without any further modification.

### 3.2. Device Fabrication

The binary and ternary bulk heterojunction OSCs were fabricated with the inverted architecture of ITO/ZnO/active layer/$MoO_x$/Ag. The pre-patterned ITO (sheet resistance = 10 $\Omega/cm^2$) glass substrates were ultrasonicated in soap solution followed by deionized (DI) water, acetone, and then isopropyl alcohol for 20 minutes each. Then, the pre-cleaned ITO glass substrates were moved inside the ultraviolet chamber for UV-ozone treatment for 25 minutes, to remove any organic residues and to make the ITO surface hydrophilic. After performing a routine cleaning process, the zinc oxide (ZnO) electron extraction layer was deposited onto the ITO glass substrates with a thickness of about 40 nm measured by the Dektak surface profiler. The ZnO precursor solution was prepared as a previously published article [62]. The ZnO coated substrates were placed to deposit a thin layer of binary/ternary active layer. Binary blend solution of PTB7-Th as donor and $PC_{71}BM$ as acceptor was prepared with a 1:1.5 (w/w) ratio in 1,2-dichlorobenzene solution and with 3 vol% 1,8-diiodooctane used as a solvent additive. Simultaneously, the ternary solution was also prepared by adding a third non-fullerene component NAI-FN-NAI (BO). The weight ratios of NAI-FN-NAI (BO) to $PC_{71}BM$ were 0%, 20%, 50%, and 100%. A device, having 100% NAI-FN-NAI (BO) small molecule is a binary device having 0% of $PC_{71}BM$. The blend solutions were spin-coated on ZnO films at 1000 RPM for 90 seconds to fabricate the active layers and then dried in a nitrogen environment at room temperature for one hour. Subsequently, the active layer coated substrates were transferred to the thermal evaporator at a chamber pressure of □ $3 \times 10^{-6}$ mbar. To complete the device fabrication, a hole extraction layer, $MoO_x$ (□ 7 nm) and Ag (□ 70 nm), as the top electrode, were thermally evaporated using a shadow mask. The active area of the device was measured approximately to be 9 $mm^2$.

## 4. Conclusions

Here, NF in combination with $PC_{71}BM$ in ternary OSC device produces a significant enhancement in the power conversion efficiency (by □ 35%) which can be attributed to the synergistic effect of complementary absorption of the third component (NF) in the ternary devices, improved band alignment, and nano-scale morphology enhancement. The incorporation of NF strengthens the light-harvesting in the visible region enhancing the short-circuit current density ($J_{sc}$). The NAI-FN-NAI (BO), NF acceptor-based binary device shows negligible performance due to the crystalline nature of NF molecules generating high roughness in the thin film. The IS analysis provides evidence for improved charge collection efficiency as a result of introduction of NF acceptor. Owing to the formation of PTB7-

Th:NAI-FN-NAI(BO):$PC_{71}BM$ ternary blend photoactive layer at room temperature in the ambient environment, it has potential applications in realizing air-stable flexible OSCs.

**Conflicts of interest**

There are no conflicts to declare.

**Acknowledgments**

LK and SBS have contributed equally. Thu Trang Do is thankful to QUT for a QUTPRA scholarship to conduct his research. PS is thankful to QUT for the financial support from the Australian Research Council (ARC) for the Future Fellowship (Grant No. FT130101337) and QUT core funding (Grant No. QUT/322120-0301/07). SPS is thankful to the financial support from the DST-SERI/S-127 grant.

**References**


(1) Søndergaard, R.; Hösel, M.; Angmo, D.; Larsen-Olsen, T. T.; Krebs, F. C. Roll-to-Roll Fabrication of Polymer Solar Cells. *Materials Today* **2012**, *15* (1–2), 36–49. https://doi.org/10.1016/S1369-7021(12)70019-6.

(2) Sun, Y.; Chang, M.; Meng, L.; Wan, X.; Gao, H.; Zhang, Y.; Zhao, K.; Sun, Z.; Li, C.; Liu, S.; Wang, H.; Liang, J.; Chen, Y. Flexible Organic Photovoltaics Based on Water-Processed Silver Nanowire Electrodes. *Nature Electronics* **2019**, *2* (11), 513–520. https://doi.org/10.1038/s41928-019-0315-1.

(3) Cui, Y.; Yao, H.; Hong, L.; Zhang, T.; Tang, Y.; Lin, B.; Xian, K.; Gao, B.; An, C.; Bi, P.; Ma, W.; Hou, J. Organic Photovoltaic Cell with 17% Efficiency and Superior Processability. *National Science Review* **2020**, *7* (7), 1239–1246. https://doi.org/10.1093/nsr/nwz200.

(4) Cui, Y.; Wang, Y.; Bergqvist, J.; Yao, H.; Xu, Y.; Gao, B.; Yang, C.; Zhang, S.; Inganäs, O.; Gao, F.; Hou, J. Wide-Gap Non-Fullerene Acceptor Enabling High-Performance Organic Photovoltaic Cells for Indoor Applications. *Nature Energy* **2019**, *4* (9), 768–775. https://doi.org/10.1038/s41560-019-0448-5.

(5) Ganesan, S.; Mehta, S.; Gupta, D. Fully Printed Organic Solar Cells - A Review of Techniques, Challenges and Their Solutions. *Opto-electronics Review* **2019**, *27* (3), 298–320. https://doi.org/10.1016/j.opelre.2019.09.002.

(6) Qin, F.; Wang, W.; Sun, L.; Jiang, X.; Hu, L.; Xiong, S.; Liu, T.; Dong, X.; Li, J.; Jiang, Y.; Hou, J.; Fukuda, K.; Someya, T.; Zhou, Y. Robust Metal Ion-Chelated Polymer Interfacial Layer for Ultraflexible Non-Fullerene Organic Solar Cells. *Nature Communications* **2020**, *11* (1), 1–8. https://doi.org/10.1038/s41467-020-18373-0.

(7) Qin, F.; Sun, L.; Chen, H.; Liu, Y.; Lu, X.; Wang, W.; Liu, T.; Dong, X.; Jiang, P.; Jiang, Y.; Wang, L.; Zhou, Y. 54 Cm2 Large-Area Flexible Organic Solar Modules with Efficiency Above 13%. *Advanced Materials* **2021**, *33* (39), 1–8. https://doi.org/10.1002/adma.202103017.

(8) Corzo, D.; Almasabi, K.; Bihar, E.; Macphee, S.; Rosas-Villalva, D.; Gasparini, N.; Inal, S.; Baran, D. Digital Inkjet Printing of High-Efficiency Large-Area Nonfullerene Organic Solar Cells. *Advanced Materials Technologies* **2019**, *4* (7), 1–9. https://doi.org/10.1002/admt.201900040.

(9) Chen, X.; Xu, G.; Zeng, G.; Gu, H.; Chen, H.; Xu, H.; Yao, H.; Li, Y.; Hou, J.; Li, Y. Realizing Ultrahigh Mechanical Flexibility and >15% Efficiency of Flexible Organic Solar Cells via a "Welding" Flexible Transparent Electrode. *Advanced Materials* **2020**, *32* (14), 1–10. https://doi.org/10.1002/adma.201908478.

(10) Langley, D.; Giusti, G.; Mayousse, C.; Celle, C.; Bellet, D.; Simonato, J. P. Flexible Transparent Conductive Materials Based on Silver Nanowire Networks: A Review. *Nanotechnology* **2013**, *24* (45). https://doi.org/10.1088/0957-4484/24/45/452001.

(11) Zhang, H.; Wang, X.; Yang, L.; Zhang, S.; Zhang, Y.; He, C.; Ma, W.; Hou, J. Improved Domain Size and Purity Enables Efficient All-Small-Molecule Ternary Solar Cells. *Advanced Materials* **2017**, *29* (42), 1703777. https://doi.org/10.1002/adma.201703777.

(12) Li, J.; Ong, K.-H.; Sonar, P.; Lim, S.-L.; Ng, G.-M.; Wong, H.-K.; Tan, H.-S.; Chen, Z.-K. Design and Modification of Three-Component Randomly Incorporated Copolymers for High Performance Organic Photovoltaic Applications. *Polym. Chem.* **2013**, *4* (3), 804–811. https://doi.org/10.1039/C2PY20763J.

(13) Liu, G.; Jia, J.; Zhang, K.; Jia, X.; Yin, Q.; Zhong, W.; Li, L.; Huang, F.; Cao, Y. 15% Efficiency Tandem Organic Solar Cell Based on a Novel Highly Efficient Wide- Bandgap Nonfullerene Acceptor with Low Energy Loss. *Advanced Energy Materials* **2019**, *9* (11), 1803657. https://doi.org/10.1002/aenm.201803657.

(14) Meng, L.; Yi, Y.; Wan, X.; Zhang, Y.; Ke, X.; Kan, B.; Wang, Y.; Xia, R.; Yip, H.; Li, C.; Chen, Y. A Tandem Organic Solar Cell with PCE of 14.52% Employing Subcells with the Same Polymer Donor and Two Absorption Complementary Acceptors. *Advanced Materials* **2019**, *31* (18), 1804723. https://doi.org/10.1002/adma.201804723.

(15) Meng, L.; Zhang, Y.; Wan, X.; Li, C.; Zhang, X.; Wang, Y.; Ke, X.; Xiao, Z.; Ding, L.; Xia, R.; Yip, H.-L.; Cao, Y.; Chen, Y. Organic and Solution-Processed Tandem Solar Cells with 17.3% Efficiency. *Science* **2018**, *361* (6407), 1094–1098. https://doi.org/10.1126/science.aat2612.

(16) Bi, P.; Hao, X. Versatile Ternary Approach for Novel Organic Solar Cells: A Review. *Solar RRL* **2019**, *3* (1), 1–34. https://doi.org/10.1002/solr.201800263.

(17) Dong, X.; Shi, P.; Sun, L.; Li, J.; Qin, F.; Xiong, S.; Liu, T.; Jiang, X.; Zhou, Y. Flexible Nonfullerene Organic Solar Cells Based on Embedded Silver Nanowires with an Efficiency up to 11.6%. *Journal of Materials Chemistry A* **2019**, *7* (5), 1989–1995. https://doi.org/10.1039/c8ta11378e.

(18) Lu, L.; Kelly, M. A.; You, W.; Yu, L. Status and Prospects for Ternary Organic Photovoltaics. *Nature Photonics* **2015**, *9* (8), 491–500. https://doi.org/10.1038/nphoton.2015.128.

(19) Ko, S.-J.; Lee, W.; Choi, H.; Walker, B.; Yum, S.; Kim, S.; Shin, T. J.; Woo, H. Y.; Kim, J. Y. Improved Performance in Polymer Solar Cells Using Mixed PC 61 BM/PC 71 BM Acceptors. *Advanced Energy Materials* **2015**, *5* (5), 1401687. https://doi.org/10.1002/aenm.201401687.

(20) Cheng, P.; Li, Y.; Zhan, X. Efficient Ternary Blend Polymer Solar Cells with Indene-C60 Bisadduct as an Electron-Cascade Acceptor. *Energy & Environmental Science* **2014**, *7* (6), 2005. https://doi.org/10.1039/c3ee44202k.

(21) Li, H.; Lu, K.; Wei, Z. Polymer/Small Molecule/Fullerene Based Ternary Solar Cells. *Advanced Energy Materials* **2017**, *7* (17), 1602540. https://doi.org/10.1002/aenm.201602540.

(22) Xiao, L.; Liang, T.; Gao, K.; Lai, T.; Chen, X.; Liu, F.; Russell, T. P.; Huang, F.; Peng, X.; Cao, Y. Ternary Solar Cells Based on Two Small Molecule Donors with Same Conjugated Backbone: The Role of Good Miscibility and Hole Relay Process. *ACS Applied Materials & Interfaces* **2017**, *9* (35), 29917–29923. https://doi.org/10.1021/acsami.7b07960.

(23) Zhang, J.; Jiang, K.; Yang, G.; Ma, T.; Liu, J.; Li, Z.; Lai, J. Y. L.; Ma, W.; Yan, H. Tuning Energy Levels without Negatively Affecting Morphology: A Promising Approach to Achieving Optimal Energetic Match and Efficient Nonfullerene Polymer Solar Cells. *Advanced Energy Materials* **2017**, *7* (15), 1602119. https://doi.org/10.1002/aenm.201602119.

(24) Lu, L.; Chen, W.; Xu, T.; Yu, L. High-Performance Ternary Blend Polymer Solar Cells Involving Both Energy Transfer and Hole Relay Processes. *Nature Communications* **2015**, *6* (1), 7327. https://doi.org/10.1038/ncomms8327.

(25) Zhang, J.; Zhang, Y.; Fang, J.; Lu, K.; Wang, Z.; Ma, W.; Wei, Z. Conjugated Polymer–Small Molecule Alloy Leads to High Efficient Ternary Organic Solar Cells. *Journal of the American Chemical Society* **2015**, *137* (25), 8176–8183. https://doi.org/10.1021/jacs.5b03449.

(26) Zhang, Y.; Deng, D.; Lu, K.; Zhang, J.; Xia, B.; Zhao, Y.; Fang, J.; Wei, Z. Synergistic Effect of Polymer and Small Molecules for High-Performance Ternary Organic Solar Cells. *Advanced Materials* **2015**, *27* (6), 1071–1076. https://doi.org/10.1002/adma.201404902.

(27) Nielsen, C. B.; Holliday, S.; Chen, H.-Y.; Cryer, S. J.; McCulloch, I. Non-Fullerene Electron Acceptors for Use in Organic Solar Cells. *Accounts of Chemical Research* **2015**, *48* (11), 2803–2812. https://doi.org/10.1021/acs.accounts.5b00199.

(28) Guldi, D. M.; Illescas, B. M.; Atienza, C. M.; Wielopolski, M.; Martín, N. Fullerene for Organic Electronics. *Chemical Society Reviews* **2009**, *38* (6), 1587. https://doi.org/10.1039/b900402p.

(29) He, Y.; Li, Y. Fullerene Derivative Acceptors for High Performance Polymer Solar Cells. *Phys. Chem. Chem. Phys.* **2011**, *13* (6), 1970–1983. https://doi.org/10.1039/C0CP01178A.
(30) Yang, L.; Zhou, H.; Price, S. C.; You, W. Parallel-like Bulk Heterojunction Polymer Solar Cells. *Journal of the American Chemical Society* **2012**, *134* (12), 5432–5435. https://doi.org/10.1021/ja211597w.
(31) Wang, B.; Fu, Y.; Yan, C.; Zhang, R.; Yang, Q.; Han, Y.; Xie, Z. Insight Into the Role of PC71BM on Enhancing the Photovoltaic Performance of Ternary Organic Solar Cells. *Frontiers in Chemistry* **2018**, *6* (JUN), 1–8. https://doi.org/10.3389/fchem.2018.00198.
(32) Nian, L.; Kan, Y.; Wang, H.; Gao, K.; Xu, B.; Rong, Q.; Wang, R.; Wang, J.; Liu, F.; Chen, J.; Zhou, G.; Russell, T. P.; Jen, A. K. Y. Ternary Non-Fullerene Polymer Solar Cells with 13.51% Efficiency and a Record-High Fill Factor of 78.13%. *Energy & Environmental Science* **2018**, *11* (12), 3392–3399. https://doi.org/10.1039/C8EE01564C.
(33) Koppe, M.; Egelhaaf, H.-J.; Dennler, G.; Scharber, M. C.; Brabec, C. J.; Schilinsky, P.; Hoth, C. N. Near IR Sensitization of Organic Bulk Heterojunction Solar Cells: Towards Optimization of the Spectral Response of Organic Solar Cells. *Advanced Functional Materials* **2010**, *20* (2), 338–346. https://doi.org/10.1002/adfm.200901473.
(34) Chen, Y.; Qin, Y.; Wu, Y.; Li, C.; Yao, H.; Liang, N.; Wang, X.; Li, W.; Ma, W.; Hou, J. From Binary to Ternary: Improving the External Quantum Efficiency of Small-Molecule Acceptor-Based Polymer Solar Cells with a Minute Amount of Fullerene Sensitization. *Advanced Energy Materials* **2017**, *7* (17), 1700328. https://doi.org/10.1002/aenm.201700328.
(35) Li, H.; Zhang, Z.-G.; Li, Y.; Wang, J. Tunable Open-Circuit Voltage in Ternary Organic Solar Cells. *Applied Physics Letters* **2012**, *101* (16), 163302. https://doi.org/10.1063/1.4761246.
(36) Yu, R.; Yao, H.; Hou, J. Recent Progress in Ternary Organic Solar Cells Based on Nonfullerene Acceptors. *Advanced Energy Materials* **2018**, *8* (28), 1702814. https://doi.org/10.1002/aenm.201702814.
(37) Wu, J.; Li, G.; Fang, J.; Guo, X.; Zhu, L.; Guo, B.; Wang, Y.; Zhang, G.; Arunagiri, L.; Liu, F.; Yan, H.; Zhang, M.; Li, Y. Random Terpolymer Based on Thiophene-Thiazolothiazole Unit Enabling Efficient Non-Fullerene Organic Solar Cells. *Nature Communications* **2020**, *11* (1), 1–9. https://doi.org/10.1038/s41467-020-18378-9.
(38) Chang, L.; Sheng, M.; Duan, L.; Uddin, A. Ternary Organic Solar Cells Based on Non-Fullerene Acceptors: A Review. *Organic Electronics* **2021**, *90* (December 2020), 106063. https://doi.org/10.1016/j.orgel.2021.106063.
(39) Do, T. T.; Pham, H. D.; Manzhos, S.; Bell, J. M.; Sonar, P. Molecular Engineering Strategy for High Efficiency Fullerene-Free Organic Solar Cells Using Conjugated 1,8-Naphthalimide and Fluorenone Building Blocks. *ACS Applied Materials & Interfaces* **2017**, *9* (20), 16967–16976. https://doi.org/10.1021/acsami.6b16395.
(40) Xu, L.; Lee, Y.-J.; Hsu, J. W. P. Charge Collection in Bulk Heterojunction Organic Photovoltaic Devices: An Impedance Spectroscopy Study. *Applied Physics Letters* **2014**, *105* (12), 123904. https://doi.org/10.1063/1.4896633.
(41) Zhou, Y.; Fuentes-Hernandez, C.; Shim, J.; Meyer, J.; Giordano, A. J.; Li, H.; Winget, P.; Papadopoulos, T.; Cheun, H.; Kim, J.; Fenoll, M.; Dindar, A.; Haske, W.; Najafabadi, E.; Khan, T. M.; Sojoudi, H.; Barlow, S.; Graham, S.; Brédas, J.-L.; Marder, S. R.; Kahn, A.; Kippelen, B. A Universal Method to Produce Low–Work Function Electrodes for Organic Electronics. *Science* **2012**, *336* (6079), 327–332. https://doi.org/10.1126/science.1218829.
(42) Do, T.-T.; Subbiah, J.; Manzhos, S.; Jones, D. J.; Bell, J. M.; Sonar, P. Phthalimide and Naphthalimide: Effect of End-Capping Groups on Molecular Properties and Photovoltaic Performance of 9-Fluorenone Based Acceptors for Organic Solar Cells. *Organic Electronics* **2018**, *62*, 12–20. https://doi.org/10.1016/j.orgel.2018.06.040.

(43) Liao, S.-H.; Jhuo, H.-J.; Cheng, Y.-S.; Chen, S.-A. Fullerene Derivative-Doped Zinc Oxide Nanofilm as the Cathode of Inverted Polymer Solar Cells with Low-Bandgap Polymer (PTB7-Th) for High Performance. *Adv. Mater.* **2013**, *25* (34), 4766–4771. https://doi.org/10.1002/adma.201301476.
(44) Wallace, A. M.; Curiac, C.; Delcamp, J. H.; Fortenberry, R. C. Accurate Determination of the Onset Wavelength ( λ Onset ) in Optical Spectroscopy. *Journal of Quantitative Spectroscopy and Radiative Transfer* **2021**, *265*, 107544. https://doi.org/10.1016/j.jqsrt.2021.107544.
(45) Xie, Y.; Yang, F.; Li, Y.; Uddin, M. A.; Bi, P.; Fan, B.; Cai, Y.; Hao, X.; Woo, H. Y.; Li, W.; Liu, F.; Sun, Y. Morphology Control Enables Efficient Ternary Organic Solar Cells. *Advanced Materials* **2018**, *30* (38), 1803045. https://doi.org/10.1002/adma.201803045.
(46) Mai, J.; Lau, T.-K.; Xiao, T.; Su, C.-J.; Jeng, U.; Zhao, N.; Xiao, X.; Lu, X. Ternary Morphology Facilitated Thick-Film Organic Solar Cell. *RSC Advances* **2015**, *5* (107), 88500–88507. https://doi.org/10.1039/C5RA17268C.
(47) Tang, B.; Liu, J.; Cao, X.; Zhao, Q.; Yu, X.; Zheng, S.; Han, Y. Restricting the Liquid–Liquid Phase Separation of PTB7-Th:PF12TBT:PC 71 BM by Enhanced PTB7-Th Solution Aggregation to Optimize the Interpenetrating Network. *RSC Advances* **2017**, *7* (29), 17913–17922. https://doi.org/10.1039/C6RA28306C.
(48) Do, T.-T.; Takeda, Y.; Manzhos, S.; Bell, J.; Tokito, S.; Sonar, P. Naphthalimide End Capped Anthraquinone Based Solution-Processable n-Channel Organic Semiconductors: Effect of Alkyl Chain Engineering on Charge Transport. *Journal of Materials Chemistry C* **2018**, *6* (14), 3774–3786. https://doi.org/10.1039/C7TC05172G.
(49) Srivastava, S. B.; Sonar, P.; Singh, S. P. Charge Transport Studies in Donor-Acceptor Block Copolymer PDPP-TNT and PC71BM Based Inverted Organic Photovoltaic Devices Processed in Room Conditions. *AIP Advances* **2015**, *5* (7), 077177. https://doi.org/10.1063/1.4927763.
(50) Bisquert, J.; Garcia-Belmonte, G.; Bueno, P.; Longo, E.; Bulhões, L. O. S. Impedance of Constant Phase Element (CPE)-Blocked Diffusion in Film Electrodes. *Journal of Electroanalytical Chemistry* **1998**, *452* (2), 229–234. https://doi.org/10.1016/S0022-0728(98)00115-6.
(51) Bisquert, J. Interpretation of Electron Diffusion Coefficient in Organic and Inorganic Semiconductors with Broad Distributions of States. *Physical Chemistry Chemical Physics* **2008**, *10* (22), 3175. https://doi.org/10.1039/b719943k.
(52) Srivastava, S. B.; Sonar, P.; Singh, S. P. Analysis of Degradation Mechanisms in Donor–Acceptor Copolymer Based Organic Photovoltaic Devices Using Impedance Spectroscopy. *Materials Research Express* **2016**, *3* (9), 096202. https://doi.org/10.1088/2053-1591/3/9/096202.
(53) Chen, B.; Qiao, X.; Liu, C.-M.; Zhao, C.; Chen, H.-C.; Wei, K.-H.; Hu, B. Effects of Bulk and Interfacial Charge Accumulation on Fill Factor in Organic Solar Cells. *Applied Physics Letters* **2013**, *102* (19), 193302. https://doi.org/10.1063/1.4805053.
(54) Qi, B.; Wang, J. Fill Factor in Organic Solar Cells. *Physical Chemistry Chemical Physics* **2013**, *15* (23), 8972. https://doi.org/10.1039/c3cp51383a.
(55) Bisquert, J.; Mora-Seró, I. Simulation of Steady-State Characteristics of Dye-Sensitized Solar Cells and the Interpretation of the Diffusion Length. *The Journal of Physical Chemistry Letters* **2010**, *1* (1), 450–456. https://doi.org/10.1021/jz900297b.
(56) Garcia-Belmonte, G.; Guerrero, A.; Bisquert, J. Elucidating Operating Modes of Bulk-Heterojunction Solar Cells from Impedance Spectroscopy Analysis. *The Journal of Physical Chemistry Letters* **2013**, *4* (6), 877–886. https://doi.org/10.1021/jz302064z.
(57) Baumann, A.; Lorrmann, J.; Rauh, D.; Deibel, C.; Dyakonov, V. A New Approach for Probing the Mobility and Lifetime of Photogenerated Charge Carriers in Organic Solar Cells

Under Real Operating Conditions. *Adv. Mater.* **2012**, *24* (32), 4381–4386. https://doi.org/10.1002/adma.201200874.

(58) Ameri, T.; Khoram, P.; Min, J.; Brabec, C. J. Organic Ternary Solar Cells: A Review. *Advanced Materials* **2013**, *25* (31), 4245–4266. https://doi.org/10.1002/adma.201300623.

(59) Diao, Y.; Zhou, Y.; Kurosawa, T.; Shaw, L.; Wang, C.; Park, S.; Guo, Y.; Reinspach, J. A.; Gu, K.; Gu, X.; Tee, B. C. K.; Pang, C.; Yan, H.; Zhao, D.; Toney, M. F.; Mannsfeld, S. C. B.; Bao, Z. Flow-Enhanced Solution Printing of All-Polymer Solar Cells. *Nature Communications* **2015**, *6*, 1–10. https://doi.org/10.1038/ncomms8955.

(60) Zhang, M.; Zhang, F.; An, Q.; Sun, Q.; Wang, W.; Zhang, J.; Tang, W. Highly Efficient Ternary Polymer Solar Cells by Optimizing Photon Harvesting and Charge Carrier Transport. *Nano Energy* **2016**, *22*, 241–254. https://doi.org/10.1016/j.nanoen.2016.02.032.

(61) Duan, L.; Zhang, Y.; Deng, R.; Yi, H.; Uddin, A. Balance between Energy Transfer and Exciton Separation in Ternary Organic Solar Cells with Two Conjugated Polymer Donors. *ACS Appl. Energy Mater.* **2020**, *3* (6), 5792–5803. https://doi.org/10.1021/acsaem.0c00740.

(62) Srivastava, S. B.; Srivastava, S. K.; Singh, S. P. Molecular-Shape-Induced Efficiency Enhancement in PC 61 BM and PC 71 BM Based Ternary Blend Organic Solar Cells. *The Journal of Physical Chemistry C* **2017**, *121* (32), 17104–17111. https://doi.org/10.1021/acs.jpcc.7b04425.

# Table of Content (ToC)

Owing to the synergistic effect of complementary absorption, band alignment, and nano-scale morphology enhancement, a non-fullerene small molecule NAI-FN-NAI (BO) as the third component in a ternary system with the host blend based on a donor polymer (PTB7-Th) and fullerene derivative ($PC_{71}BM$) exhibits the power conversion efficiency of 8.1%, which is ~35% higher than the efficiency of PTB7-Th:$PC_{71}BM$ binary OSC.